Mechanics Research Communications 54 (2013) 14–20

Contents lists available at ScienceDirect

Mechanics Research Communications

journal homepage: www.elsevier.com/locate/mechrescom

Rapid evaluation of the fatigue limit in composites using infrared lock-in thermography and acoustic emission

E.Z. Kordatos [a], K.G. Dassios [a], D.G. Aggelis [a,b], T.E. Matikas [a,*]

[a] Department of Materials Science and Engineering, University of Ioannina, 45110 Ioannina, Greece
[b] Department of Mechanics of Materials and Constructions, Vrije Universiteit Brussel, Pleinlaan 2, 1050 Brussels, Belgium

ARTICLE INFO

Article history:
Received 15 December 2012
Received in revised form 10 May 2013
Accepted 16 September 2013
Available online xxx

Keywords:
Fatigue limit
Lock-in thermography
Acoustic emission
CMC

ABSTRACT

Fatigue limit determination via the conventional Wöhler-curve method is associated with extended experimental times as it requires testing of a large number of specimens. The current paper introduces a methodology for fast, reliable and experimentally economic determination of the fatigue limit in monolithic and composite materials by means of combined usage of two nondestructive inspection methods, namely infrared (IR) lock-in thermography and acoustic emission (AE). IR thermography, as a real-time and non-contact technique, allowed the detection of heat waves generated due to thermo-mechanical coupling as well as of the energy dissipated intrinsically during dynamic loading of the material. AE, on the other hand, was employed to record the transient waves resulting from crack propagation events. Aluminum grade 1050 H16 and cross-ply SiC/BMAS ceramic matrix composites were subjected to fatigue loading at various stress levels and were monitored by an IR camera and AE sensors. The fatigue limit of the monolithic material, obtained by the lock-in infrared thermography technique and supported by acoustic emission was found to be in agreement with measurements obtained by the conventional S–N curve method. The fatigue limit of the ceramic matrix composite was validated with acoustic emission data.

1. Introduction

High temperature aerospace applications require materials with advanced thermo-mechanical properties. Since their development nearly two decades ago, ceramic matrix composites (CMCs) have been fulfilling this need in applications including gas turbine parts, jet motor nozzles, thermal barriers, internal chambers and aircraft brakes. Among the various CMC constituents, the barium osumilite ($BaMg_2Al_6Si_9O_{30}$, BMAS: barium–magnesium–alumina–silicate) matrix system (Brennan, USA patent No.: 4589900, 1986), is widely known for its good thermo-physical (Choy et al., 2000) and mechanical properties (Johnson et al., 1987; Yilmaz and Taylor, 2007) while SiC fibers are specially known for their thermal stability, high-temperature mechanical performance and strength, providing CMCs with remarkable mechanical properties (Brennan and Prewo, 1982).

In the aerospace industry, inspection is of great significance in all fabrication stages. The non-destructive assessment of a structure in the prototype stage of mechanical design allows the option of choice of the appropriate component characteristics that will ensure the optimal performance during the operational phase. Non-destructive methodologies have been applied in the past to assess damage formation and propagation in real testing time in various material systems (Dassios and Galiotis, 2006; Kim and Liaw, 2007; Kordatos et al., 2013; Mei et al., 2007; Sfarra et al., 2010).

Despite the considerable technological advances in NDE instrumentation and processing power, quick and reliable non-destructive assessment techniques are still an open challenge. Infrared thermography (IRT) is a real-time, fast and full-field inspection tool that has proven capable of satisfying this necessity. IRT has been efficiency used to assess the thermo-mechanical behavior of a wide range of materials and structures such as carbon steels (Kordatos and Matikas, 2011), aluminum alloys (Kordatos et al., 2012), steel-fiber reinforced concrete (Aggelis et al., 2010), metal matrix composites (MMCs) (Kordatos et al., 2012) and CMCs (Dassios et al., 2013; Kim and Liaw, 2007).

Among the most important mechanical performance indicators for aerospace materials is their fatigue behavior. The fatigue limit, a key property of the dynamic performance of a material, is conventionally determined using the “Wöhler curve” or “S–N curve” approach, a plot of the magnitude of a cyclic stress (S) against the logarithmic scale of cycles to failure (N). The particular method is time consuming as it requires testing a large number of specimens at different load levels. Newly developed IRT-based methodologies overcome this fundamental limitation and facilitate the rapid determination of the fatigue limit by

* Corresponding author. Tel.: +30 26510 07216; fax: +30 26510 08054.
E-mail address: matikas@otenet.gr (T.E. Matikas).

0093-6413/$ – see front matter © 2013 Elsevier Ltd. All rights reserved.
http://dx.doi.org/10.1016/j.mechrescom.2013.09.005

narrowing the required experimental time in the order of one day or less. Risitano et al. (Fargione et al., 2002; La Rosa and Risitano, 2000) developed a thermographic methodology to establish the fatigue limit and construct the S–N curve. The "Thermographic Method (TM)" or "Risitano Method" is based on the analysis of the surface temperature of a specimen subjected to cyclic loading. The material's dissipativity can also be useful in the determination of the fatigue limit (Luong, 1998). Luong (Luong, 1995; Minh Phong, 1998) developed a methodology for the rapid evaluation of the fatigue strength of metals based on the detection of the occurrence of intrinsically dissipated energy from the fatigue-loaded material. Based on the Luong approach, Bremond and Potet (2001) developed the "D-Mode" technique, a digital processing methodology which allows the extracting of non-linear coupled thermo-mechanical effects per cycle to determine the endurance limit of the materials.

The aforementioned methods have been applied for the non-destructive assessment of the fatigue limits of various materials, such as steel (Curà et al., 2005; Krapez and Pacou, 2002; Krapez et al., 2000), aluminum (Krapez and Pacou, 2002; Krapez et al., 2000), and concrete (Luong, 2000). Moreover, complex structures (Arnould et al., 2005), riveted components (Li et al., 2012) and butt-welded AH36 steel joints (Crupi et al., 2009) have also been studied using IRT methods.

Acoustic emission is based on the transient elastic signals emitted by the tip of the crack during propagation moments. It utilizes piezoelectric sensors mounted on the surface of the materials which record these signals and transform them in electric waveforms which are digitized and stored (Grosse and Ohtsu, 2008). The population and rate of the recorded signals as well as the waveform shape parameters have proven indicative to the severity of the damage process, and have been correlated with the crack propagation rate under fatigue (Aggelis et al., 2011; Roberts and Talebzadeh, 2003), the fracture mode (Kim et al., 2004; Ohno and Ohtsu, 2010), while the rate of incoming signals have been used to correlate with the remaining life of a material (Suzuki and Ohtsu, 2004; Dai and Labuz, 1997).

In the present study, the efficiency of IR lock-in thermography to assess the fatigue limit is tested across two materials, namely aluminum 1050, temper H16, and cross-ply SiC/BMAS glass–ceramic matrix composites. Specimens of "dog-bone" configuration were subjected to fatigue loading in various load levels and were monitored concurrently by an infrared camera and AE sensors. The aim was to investigate whether AE indices can be similarly used in the direction of evaluating the fatigue limit of the materials. To the authors' knowledge this is the first time that the fatigue limit of materials is estimated by combination of acoustic emission and thermography.

2. Experimental study

2.1. Materials

Aluminum, grade 1050 and temper H16, is strain-hardened to three quarters of the material's maximum hardness condition. Known for its good formability and ductility, the material is widely used in applications such as aluminum composite panels, curtain walls, ceiling boards and decoration materials. The mechanical properties and the chemical composition of the material are presented in Tables 1 and 2 respectively.

Cross-ply ceramic matrix composite laminates, 3 mm thick, were processed by AEA Technology (Harwell Ltd., United Kingdom). Silicon carbide, grade "Tyranno", fibers (UBE Industries Ltd., Japan) were used to reinforce the BMAS glass–ceramic matrix. The nominal elastic modulus and strength of the Tyranno fibers, as quoted by the manufacturer, are 190 GPa and 3.3 GPa respectively. The tensile strength of this material is 293 MPa (Dassios and Matikas, 2013). The main steps of the composite's manufacturing route are the following:

Table 1
Mechanical properties of aluminum 1050-H16.

Property	Value
Ultimate tensile strength, σ_{uts} (MPa)	140.081
Elongation at break, ε (%)	8
Brinell hardness, HB	35

Table 2
Chemical composition of aluminum 1050 H16.

Element	Wt%
Al	99.5 max
Si	0.25 max
Fe	0.4 max

a) Desizing of the fiber bundles in furnace
b) Wetting the desized fibers in a slurry of the precursor glass frit
c) Winding the fibers on a mandrel and allowing to dry for 20 min
d) Cutting and manually arranging the fibers in layers for the preparation of prepreg sheets
e) Stacking the sheets in (0.90) 4 s sequence
f) Burning the binder off
g) Hot pressing in a graphite die at ~1200 °C for 10 min
h) Final crystallization step at 1300 °C

2.2. Testing setup and experimental procedure

Fatigue testing was carried out on an Instron servo-hydraulic machine capable of a maximum static or dynamic load of ±100 kN. Throughout testing, the materials were monitored by an IR camera CEDIP (MIW) with a cooled indium antimonide (InSb) detector (3–5 μm). The camera has a focal plane array (FPA) with pixel format of 320 (H) × 240 (V), sensitivity of 20 mK and a frame capturing rate of 100 Hz. Optimal field-of-view (FOV) conditions were achieved by installing the IR camera at a distance of approximately 40 cm in front of the specimen (Fig. 1). The camera was connected to the lock-in amplifier which, in turn, was connected to the servo-hydraulic controller. This configuration enabled synchronization of the frequency between the lock-in amplifier and the testing machine and the collection of lock-in images and data during fatigue testing.

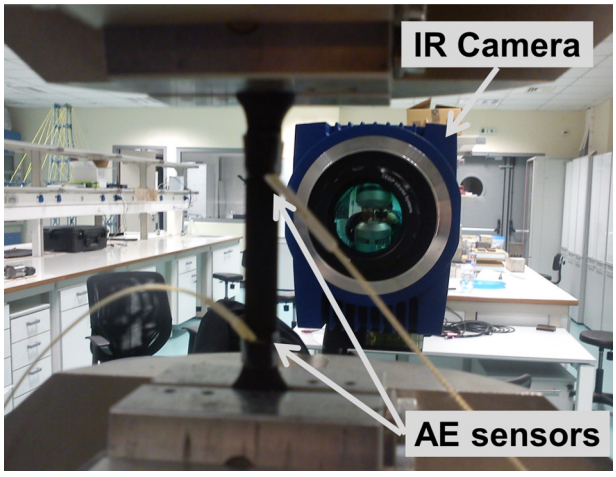

Fig. 1. Experimental setup.

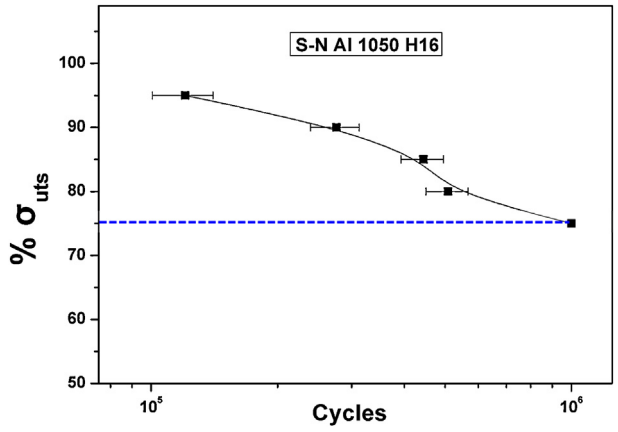

Fig. 2. Wöhler curve for the Al 1050 H16.

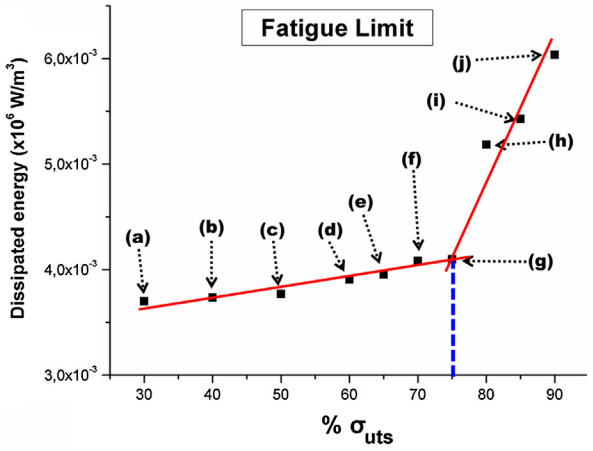

Fig. 3. Dissipated energy vs $\%\sigma_{uts}$ (Al 1050 H16).

Prior to testing, specimens were spray-coated with a matte black varnish that helped the establishment of a uniform and high-level surface emissivity. The materials were subjected to step-loading fatigue until fracture. In the first loading step, fatigue load was set at 10% of σ_{uts} for a duration of 6000 cycles. In every next five steps, amplitude was increased incrementally by 10% σ_{uts}. Beyond the 60% σ_{uts} level, fatigue load level increased by 5% of σ_{uts} up to ultimate fracture. The frequency of the sinusoidal fatigue load was 10 Hz and R was equal to 0.1.

During dynamic loading, the quantity of energy emitted as infrared radiation at the specimen surface, which is a function of the temperature and emissivity of the specimen, was captured by the IR camera. Based on Luong's approach, the measured energy is the intrinsically dissipated energy while the fatigue limit is revealed by a significant slope shift in the dissipated energy versus σ_{uts} plot of the material.

To allow for comparison of lock-in thermography results with the conventional technique, the fatigue limit of aluminum 1050 H16 was also determined via the Wöhler curve method by testing a large number of specimens. The runout of the test was defined at 10^6 cycles.

For AE monitoring, two wideband AE sensors (Pico of Physical Acoustics, PAC) were attached on one side of the specimen using silicon grease for coupling and secured by tape throughout the duration of the experiment. The particular sensors exhibit a relatively broadband response ranging from 100 to 800 kHz with a maximum sensitivity at 450 kHz. This bandwidth range enables recording of a wide variety of possible sources while their small size makes their use ideal for the small specimen sizes associated with the dog-bone configuration. The pre-amplifier gain was set at 40 dB, and the signals were recorded on a PCI-2 board of PAC with a sampling rate of 10 MHz. No extra frequency filter was applied. The distance between the sensors was 45 mm while they were attached approximately 10 mm outside the grips (see Fig. 2). In order to avoid low-intensity friction noise from the grips the threshold was set at 45 dB, while signals with "zero" energy were filtered out.

3. Results and discussion

3.1. Metal (aluminum 1050 H16)

For the purpose of benchmarking the proposed methodology, the fatigue limit of aluminum specimens was initially established using the conventional Wöhler (S–N) curve method. Five different stress levels were examined ranging from 95% σ_{uts} to 75% σ_{uts}, within the imposed "runout" level, 10^6 cycles. Five specimens for each load level were tested and the results are demonstrated in Fig. 2. The error bars correspond to one standard deviation from the mean value established among the five specimens tested. It can be observed that the fatigue limit at "runout" is 75% σ_{uts}, or 105 MPa for aluminum 1050 H16.

Fig. 3 represents the thermally dissipated energy, captured for a typical Al 1050 H16 specimen by the lock-in IRT technique, versus imposed load level ($\%\sigma_{uts}$). It is observed that energy varies as a function of $\%\sigma_{uts}$ and two distinct regimes of linear trends with different slopes are prominent. The abscissa of the point of intersection of the two linear regressions to the data within each regime, corresponds to the fatigue limit. In the particular case, the fatigue limit assessed by lock-in thermography is 75% σ_{uts}. This value, which was found not to vary significantly among different specimens, compares favorably with the results from Wöhler curve analysis presented earlier. Irrespective of the statistical repeatability of the IRT-established fatigue limit among different samples, it is important to note that its calculation can be based on test data collected from as few as one single test specimen (Fig. 3). Hence the proposed thermographic approach overcomes the limitations of large number of specimens and long experimental time associated with the conventional Wöhler curve approach.

It is relevant to discuss the above findings in view of the thermographic response of the material with respect to dynamic loading. The ten thermographs presented in Fig. 4 depict the energy dissipated by aluminum specimens under equal in number stress levels ranging from 30 to 95% σ_{uts}. Thermographs 4a, 4b and 4c correspond to 30, 40 and 50% σ_{uts} respectively and do not show notable change in dissipated energy. A small change in energy is demonstrated by increasing warmer colors (light blue to green) in thermographs 4d, 4e and 4f which correspond to σ_{uts} levels of 60%, 65% and 70%, respectively. The energy dissipation characteristics of the material change drastically at thermograph 4 g, at a load level of 75% σ_{uts} which corresponds to the fatigue limit established by the slope change in the curve of Fig. 3. From this load level and on, saturation of dislocations and microcracks occur until the final failure of the specimen. This leads to higher amounts of dissipated energy and is captured in "warmer" (red to magenta) coloring in thermographs 4h–j.

As far as AE is concerned, the current study focused on the analysis of the cumulative populations of hits. In previous studies on metals under fatigue loading, acquisition of AE hits has been seen to be continuous with a rate that may exhibit fluctuations for the duration of the fatigue block (Aggelis et al., 2011; Kim et al., 2004; Qian et al., 2009). Fig. 5 shows the typical cumulative activity recorded for an aluminum specimen as a function of time. A constant rate of emissions is observed within subsequent load levels as revealed

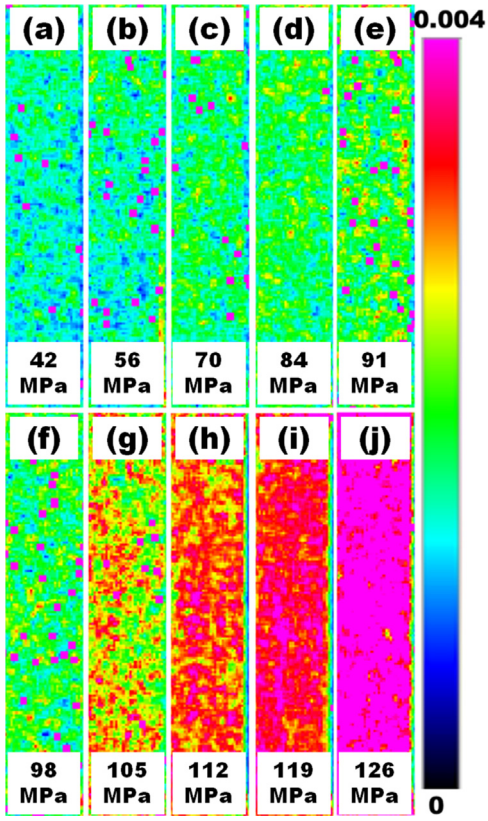

Fig. 4. Thermographs for Al 1050 H16 specimens.

by the high correlation coefficients. The inclinations (AE hit rates) exhibit fluctuations among successive levels. The strongest change is seen at the end of the loading level of 75% σ_{uts} and before the start of the next level, corresponding to 80% σ_{uts}. This strong bending point on the curve is quite close to the bend noted in the dissipated energy plot of Fig. 3. The behavior signifies that, during fatigue at levels above the fatigue limit, AE hit rate undergoes a significant increase compared to the activity at lower levels. This is attributed to the damage accumulation that takes place with a higher rate and finally leads to failure, compared to the damage accumulation at lower levels of loading. These processes do not influence the strain readings directly but can be captured by AE due to the high sensitivity of the sensors. It is characteristic that the rate between the successive cycles of 75% and 80% of σ_{uts} increases from 0.35 to

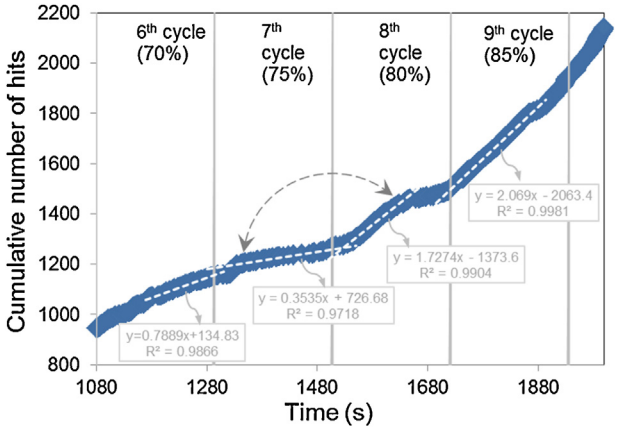

Fig. 5. Cumulative AE activity for different loading stages of aluminum specimen.

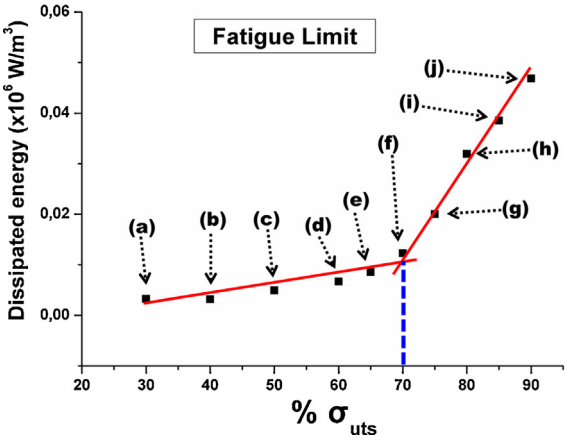

Fig. 6. Dissipated energy vs %σ_{uts} (SiC/BMAS).

1.73 hits/s, by approximately five times. This finding is indicative of the different severity of the processes that occur at the lower and the higher sides of the fatigue limit.

3.2. Ceramic matrix composite

The plausible findings for aluminum 1050 H16, challenged examination of the applicability of the IRT-based fatigue limit determination technique on materials of different nature and more complex microstructure, such as ceramic matrix composites. Fig. 6 represents the energy dissipated by a typical SiC/BMAS composite specimen as a function of 10 different imposed load levels, ranging from 30 to 90% σ_{uts}.

Similarly to the case of Al 1050 H16, the curve exhibits two distinct slopes. In the initial stress levels, ranging from 30 to 60% σ_{uts}, the dissipated energy appears to increase with a low rate, while from 70% σ_{uts} and upwards it rises in a much steeper manner. As discussed previously, the abscissa of the intersection point of the two linear regressions to the two distinct regimes provides the fatigue limit of the material. The fatigue limit calculated by the thermographic method for the cross-ply SiC/BMAS is then 70% σ_{uts}, or 205 MPa and was not found to vary significantly among different specimens.

It is interesting to examine the thermographic response of the ceramic matrix composite in view of the IRT-based fatigue limit value of 70% σ_{uts}. Fig. 7 represents typical thermographs collected at ten successive stress levels for the CMC under consideration, ranging from 30 to 90% σ_{uts}. Two distinct scenarios are, again, made evident. The initial loading levels associated with minimal material damage are depicted with “cold” color coding (low energy) in thermographs 7a–d, whereas progressive damage accumulation is captured by increasingly warmer colors (high energy) in thermographs 7e–j. This signifies that in the first four stress levels, 30–60% σ_{uts} there is no appreciable change in the dissipated energy, while at 70% σ_{uts}, thermograph 7e, a slight change in color indicates the saturation of elastic energy accumulation on the onset of appearance of fatigue. In thermograph 7f a massive energy scenario unfolds due to the action of internal energy dissipation phenomena such as matrix cracking, interfacial failure and subsequent fiber–matrix debonding, intact fiber sliding across the debonded interface, fiber bridging, fiber failure and pull-out (Dassios, 2007; Dassios et al., 2005). In thermographs 7g, 7h, 7i and 7j, corresponding to 75%, 80%, 85% and 90% σ_{uts} respectively, a raise in dissipated energy is indicated by the increase in the density of “warmer” colors (magenta spots) up to ultimate fracture. The fatigue limit of cross-ply glass–ceramic matrix

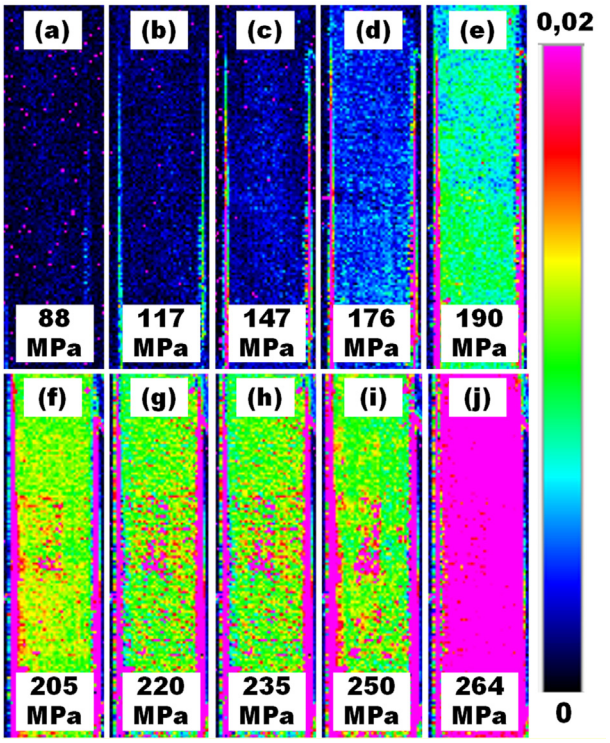

Fig. 7. Thermographs of SiC/BMAS.

composite can then be also easily determined by application of the proposed IR thermography methodology, in a short experimental time.

Results of AE monitoring during fatigue testing of SiC/BMAS specimens can be seen in Fig. 8. The rate of AE acquisition changes between different load levels while, in most cases, the different blocks can be distinguished by naked eye. In general terms, the rate follows an increasing trend, starting from approximately 1 hit/s at the early stages of 55% and 60% of the σ_{uts}, where the activity is negligible, and reaching 10 hit/s at the last level of 95% σ_{uts}. AE energy is also depicted in Fig. 8b. The particular indicator corresponds to the measured area under the rectified signal envelope (MARSE) and is related to the energy of the stress wave emitted by the source event (Anastasopoulos et al., 2009). Again, the first blocks show a weak accumulation of energy, while after the 70% loading stage, energy seems to be accumulated in a much higher rate, until the failure of the specimen.

In order to more clearly examine the trends between the AE activity and energy, their rates are normalized with respect to their maximum values (rate at final load level) and are seen in Fig. 9. A change of slope is prominent for both parameters at a load level equal to 70% σ_{uts}. Before that point, the increase of hit rate is negligible between successive steps, while the energy rate is close to zero (typically negative, due to slight fluctuations). This finding indicates that the mechanical processes occurring internally in the material are not affected by the load level, provided that this level is lower than the fatigue limit. When the fatigue amplitude increases above the fatigue limit the rate of activity becomes steadily higher and much higher energy is emitted. Both parameters (hit rate and energy) show that the change of behavior occurs after the loading amplitude of 70% of σ_{uts}. It is worth mentioning that AE energy is slightly more indicative of the mechanical state of the material than the population of hits because it is associated with a steeper slope than that of hit rate. The hits are not only generated in larger numbers during high amplitude fatigue, but also they contain higher energy following the higher intensity damage

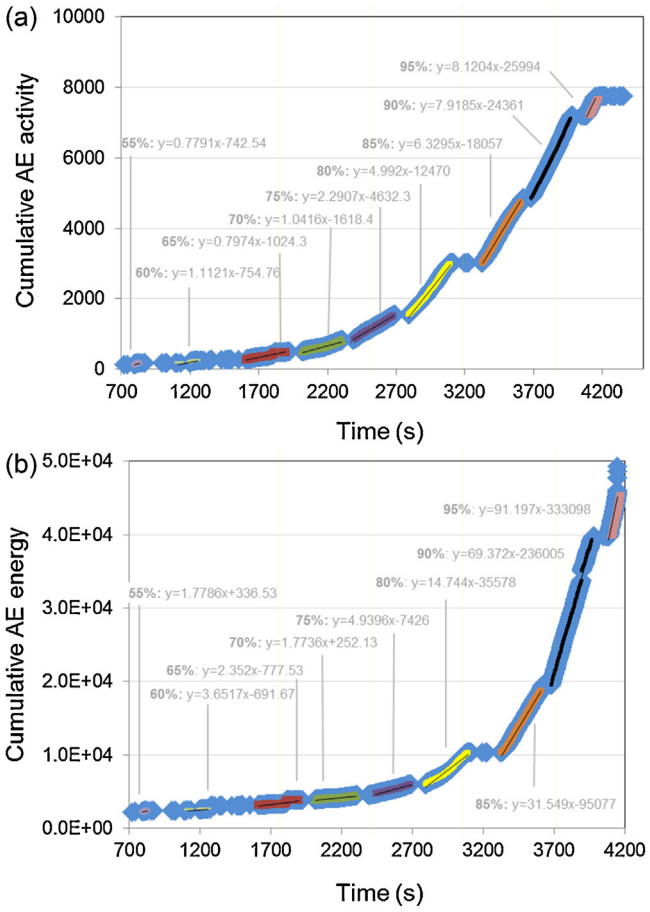

Fig. 8. Cumulative AE (a) activity and (b) energy vs time.

processes that occur at the latest stages. This shows the importance of examining qualitative AE features of AE complementary to population measurement alone, as in a number of cases the waveform parameters like the energy or the rise time has proven very indicative of processes like damage mode shifting, stress intensity factor changes and self-healing (Aggelis et al., 2011; Van Tittelboom et al., 2012; Zárate et al., 2012).

The trends presented in the two distinct regimes of Fig. 9 are clearer for the ceramic matrix composite than the monolithic material (aluminum) presented earlier in Fig. 5. This is most likely due to the heterogeneity and the complicated microstructure of the

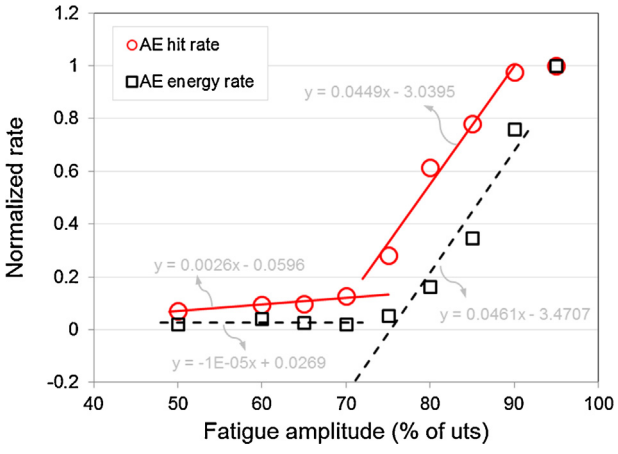

Fig. 9. Rate of increase of accumulated hits and energy.

material which consists of fibers, matrix and successive layers of 0° and 90° plies. This leads to a variety of failure mechanisms that are gradually developing (matrix cracks, delaminations, pull-out events) and results in more indications on the propagation of fracture as compared to aluminum where actually one single fracture mechanism is active for most of the fatigue life of the specimen. This shows that the AE approach for fast evaluation of the fatigue limit is even more promising for composite materials than monolithic ones. Nonetheless, it should be kept in mind that the importance of this approach lies on the changing trends (i.e. bending points on the curves) that indicate the critical shift of the intensity of damage mechanisms between loads lower and higher than the fatigue limit and not on the absolute values of the specific AE parameters. This is because the results of AE always depend on the specific setup, including the type of sensors, their separation distance, as well as the specimen geometry. Indeed, the emitted energy is in the form of elastic waves, being therefore prone to material damping, scattering on the heterogeneities and geometry dispersion due to the prismatic, waveguide-like shape of the specimens. Other parameters that have shown their potential for early characterization of damage, like the *b*-value analysis did not show monotonic trends as to the successive loading steps and thus it is not presented herein. Additionally, details like source location data are not presented either since the aim of the study is not to examine the most sensitive point of the anyway small specimen; the interest is focused on parameters that may help in the characterization of the fatigue limit.

4. Conclusions

IR lock-in thermography was found to be an effective tool for the rapid and accurate assessment of the fatigue limit of monolithic and composite materials by means of interrogation of the instances of slope change in the plots of thermally dissipated energy versus $\%\sigma_{uts}$. It was found that both rates of AE data acquisition and energy exhibited similar slope shifts trends at locations that compare favorably with their thermographic findings.

Using IR thermography, the fatigue limit of aluminum 1050 H16 was determined at 75% σ_{uts}, a value which was found in favorable agreement with that determined by the conventional Wöhler curve approach. The proposed methodology was also applied for the rapid determination of the fatigue limit, at 70% σ_{uts}, of a much more complex system, a cross-ply glass–ceramic matrix composite material. AE data also exhibited a steep change in energy and acquisition rate at 70% σ_{uts}, indicating good agreement with the thermographic assessment.

It is concluded that the determination of fatigue limit by means of IR lock-in thermography benchmarked by acoustic emission offers a new, versatile and accurate methodology that can surpass the limitations of the Wöhler's curve approach, since it significantly reduces the experimental time needed and requires as few as a single test specimen for obtaining the fatigue limit of any material.

References

Aggelis, D.G., Kordatos, E.Z., Matikas, T.E., 2011. Acoustic emission for fatigue damage characterization in metal plates. Mechanics Research Communications 38, 106–110.

Aggelis, D.G., Kordatos, E.Z., Soulioti, D.V., Matikas, T.E., 2010. Combined use of thermography and ultrasound for the characterization of subsurface cracks in concrete. Construction and Building Materials 24, 1888–1897.

Anastasopoulos, A., Kourousis, D., Botten, S., Wang, G., 2009. Acoustic emission monitoring for detecting structural defects in vessels and offshore structures. Ships and Offshore Structures 4, 363–372.

Arnould, O., Brémond, P., Hild, F., 2005. Thermal evaluation of the mean fatigue limit of a complex structure. In: Thermosense XXVII, Proceedings of the SPIE, vol. 5782, pp. 255–263.

Bremond, P., Potet, P., 2001. Lock-in thermography: a tool to analyze and locate thermomechanical mechanisms in materials and structures. In: Proceedings of SPIE 4360, Thermosense XXIII, 560 (March 23, 2001), http://dx.doi.org/10.1117/12.421039.

Brennan, J.J., Taylor, M.P., 1986. USA patent No.: 4589900. High strength thermally stable magnesium aluminosilicate glass ceramic matrix SiC fibre composite.

Brennan, J.J., Prewo, K.M., 1982. Silicon carbide fibre reinforced glass–ceramic matrix composites exhibiting high strength and toughness. Journal of Materials Science 17, 2371–2383.

Choy, K.L., Duplock, P., Rogers, P.S., Churchman-Davies, J., Pirzada, M.T., 2000. The mechanical behaviour of glass and glass–ceramic matrix composites. Materials Science and Engineering A: Structural Materials 278, 187–194.

Crupi, V., Guglielmino, E., Maestro, M., Marinò, A., 2009. Fatigue analysis of butt welded AH36 steel joints: thermographic method and design S–N curve. Marine Structures 22, 373–386.

Curà, F., Curtis, G., Sesana, R., 2005. A new iteration method for the thermographic determination of fatigue limit in steels. International Journal of Fatigue 27, 453–459.

Dai, S., Labuz, J., 1997. Damage and failure analysis of brittle materials by acoustic emission. Journal of Materials in Civil Engineering 9 (4), 200–205.

Dassios, K.G., 2007. A review of the pull-out mechanism in the fracture of brittle-matrix fibre-reinforced cowosites. Advanced Composites Letters 16, 17–24.

Dassios, K.G., Aggelis, D.G., Kordatos, E.Z., Matikas, T.E., 2013. Cyclic loading of a SiC-fiber reinforced ceramic matrix composite reveals damage mechanisms and thermal residual stress state. Composites Part A: Applied Science and Manufacturing 44, 105–113.

Dassios, K.G., Galiotis, C., 2006. Direct measurement of fiber bridging in notched glass–ceramic-matrix composites. Journal of Materials Research 21, 1150–1160.

Dassios, K.G., Kostopoulos, V., Steen, M., 2005. Intrinsic parameters in the fracture of carbon/carbon composites. Composites Science and Technology 65, 883–897.

Dassios, K.G.M., Matikas, T.E., 2013. Residual stress-related common intersection points in the mechanical behavior of ceramic matrix composites undergoing cyclic loading. Experimental Mechanics 53 (6), 1033–1038.

Fargione, G., Geraci, A., La Rosa, G., Risitano, A., 2002. Rapid determination of the fatigue curve by the thermographic method. International Journal of Fatigue 24, 11–19.

Grosse, C.U., Ohtsu, M., 2008. Acoustic Emission Testing. Springer, Heidelberg.

Johnson, L.F., Hasselman, D.P.H., Chyung, K., 1987. Effect of silicon-carbide fiber or Whisker reinforcement on the thermal-diffusivity conductivity of an osumilite glass–ceramic. Journal of the American Ceramic Society 70, C135–C138.

Kim, J., Liaw, P.K., 2007. Tensile fracture behavior of nicalon/SiC composites. Metallurgical and Materials Transactions A 38, 2203–2213.

Kim, K.B., Yoon, D.J., Jeong, J.C., Lee, S.S., 2004. Determining the stress intensity factor of a material with an artificial neural network from acoustic emission measurements. NDT and E International 37, 423–429.

Kordatos, E.Z., Aggelis, D.G., Dassios, K.G., Matikas, T.E., 2013. In-situ monitoring of damage evolution in glass matrix composites during cyclic loading using nondestructive techniques. Applied Composite Materials 2013, 1–13.

Kordatos, E.Z., Aggelis, D.G., Matikas, T.E., 2012. Monitoring mechanical damage in structural materials using complimentary NDE techniques based on thermography and acoustic emission. Composites Part B: Engineering 43, 2676–2686.

Kordatos, E.Z., Matikas, T.E., 2011. Developing damage metrics for metallic structures undergoing fatigue using real-time thermographic evaluation. In: Proceedings of SPIE 7982, Smart Sensor Phenomena, Technology, Networks, and Systems, p. 79820U.

Krapez, J.C., Pacou, D., 2002. Thermography detection of damage initiation during fatigue tests. In: Proceedings of SPIE 4710, Thermosense XXIV, 435 (March 15, 2002), http://dx.doi.org/10.1117/12.459593.

Krapez, J.C., Pacou, D., Gardette, G., 2000. Lock-in thermography and fatigue limit of metals. In: Proceedings of QIRT'2000, pp. 277–282.

La Rosa, G., Risitano, A., 2000. Thermographic methodology for rapid determination of the fatigue limit of materials and mechanical components. International Journal of Fatigue 22, 65–73.

Li, X.D., Zhang, H., Wu, D.L., Liu, X., Liu, J.Y., 2012. Adopting lock-in infrared thermography technique for rapid determination of fatigue limit of aluminum alloy riveted component and affection to determined result caused by initial stress. International Journal of Fatigue 36, 18–23.

Luong, M.P., 1995. Infrared thermographic scanning of fatigue in metals. Nuclear Engineering and Design 158, 363–376.

Luong, M.P., 1998. Fatigue limit evaluation of metals using an infrared thermographic technique. Mechanics of Materials 28, 155–163.

Luong, P.M., 2000. Nondestructive Damage Evaluation of Reinforced Concrete Structure using Infrared Thermography. Society of Photo-Optical Instrumentation Engineers, Newport Beach, CA, USA, pp. 98–107.

Mei, H., Cheng, L.F., Zhang, L.T., Fang, P., Meng, Z.X., Liu, C.D., 2007. Real-time monitoring of thermal cycling damage in ceramic matrix composites under a constant stress. Journal of the American Ceramic Society 90, 2135–2142.

Minh Phong, L., 1998. Fatigue limit evaluation of metals using an infrared thermographic technique. Mechanics of Materials 28, 155–163.

Ohno, K., Ohtsu, M., 2010. Crack classification in concrete based on acoustic emission. Construction and Building Materials 24, 2339–2346.

Qian, W., Xie, L., Huang, D., Yin, X., 2009. Pattern recognition of fatigue damage acoustic emission signal. In: Proceedings of ICMA 2009, Mechatronics and Automation, pp. 4371–4375, http://dx.doi.org/10.1109/ICMA.2009.5246614.

Roberts, T.M., Talebzadeh, M., 2003. Acoustic emission monitoring of fatigue crack propagation. Journal of Constructional Steel Research 59, 695–712.

Sfarra, S., Ibarra-Castanedo, C., Bendada, A., Maldague, X., Ambrosini, D., Paoletti, D., 2010. Comparative study for the nondestructive testing of advanced ceramic materials by infrared thermography and holographic interferometry. In: Proceedings of SPIE 7661, Thermosense XXXII, p. 76610Q, http://dx.doi.org/10.1117/12.850742.

Suzuki, T., Ohtsu, M., 2004. Quantitative damage evaluation of structural concrete by a compression test based on AE rate process analysis. Construction and Building Materials 18, 197–202.

Van Tittelboom, K., De Belie, N., Lehmann, F., Grosse, C.U., 2012. Acoustic emission analysis for the quantification of autonomous crack healing in concrete. Construction and Building Materials 28, 333–341.

Yilmaz, R., Taylor, R., 2007. Effect of heat treatment in air on the thermal properties of SiC fibre-reinforced composite. Part 1: a barium osumilite (BMAS) matrix glass ceramic composite. Journal of Materials Science 42, 763–771.

Zárate, B., Caicedo, J., Yu, J., Ziehl, P., 2012. Probabilistic prognosis of fatigue crack growth using acoustic emission data. Journal of Engineering Mechanics 138, 1101–1111.